Robotica (2019) volume 37, pp. 141–160. © Cambridge University Press 2018
doi:10.1017/S0263574718000899

Position analysis, singularity loci and workspace of a novel 2PRPU Schoenflies-motion generator

Henrique Simas† and Raffaele Di Gregorio‡,*

†*Raul Guenther Lab. of Applied Robotics, Department of Mechanical Engineering, Federal University of Santa Catarina, Florianópolis, SC 88040–900, Brazil*
‡*Department of Engineering, University of Ferrara, Via Saragat, 1, Ferrara 44100, Italy*

(Accepted August 9, 2018. First published online: September 10, 2018)

SUMMARY
Pick-and-place applications need to perform rigid body displacements that combine translations along three independent directions and rotations around one fixed direction (Schoenflies motions). Such displacements constitute a four-dimensional (4-D) subgroup (Schoenflies subgroup) of the 6-D displacement group. The four-degrees of freedom (dof) manipulators whose end effector performs only Schoenflies motions are named Schoenflies-motion generators (SMGs). The most known SMGs are the serial robots named SCARA. In the literature, parallel manipulators (PMs) have also been proposed as SMGs. Here, a novel single-loop SMG of type 2PRPU is studied. Its position analysis, singularity loci and workspace are addressed to provide simple analytic and geometric tools that are useful for the design. The proposed single-loop SMG is not overconstrained, its actuators are on or near the base and its end effector can perform a complete rotation. These features solve the main drawbacks that parallel SMG architectures have in general and make the proposed SMG a valid design alternative.

KEYWORDS: Parallel manipulators, Schoenflies subgroup, Position analysis, Instantaneous kinematics, Workspace

1. Introduction

A number of industrial applications (e.g., pick-and-place tasks) require rigid body translations along three independent directions together with rotations around one fixed direction. The displacement set of this type constitutes the four-dimensional (4-D) Schoenflies subgroup of the 6-D displacement group[1−3] and the 4-degrees of freedom (dof) manipulators whose end effector is constrained to perform Schoenflies displacements are called Schoenflies-motion generators (SMGs).[2] The most known SMGs are the serial robots named SCARA.

In the literature (see, for instance, refs. [3-11]), parallel manipulators (PMs) have also been proposed as SMGs. Parallel architectures feature two rigid bodies, one fixed (base) and the other movable (platform), that are connected with one another by a number of kinematic chains (limbs). Most of the parallel SMGs have four limbs (e.g.[4−6,8,11]), and one actuator per limb located on the base. Nevertheless, two-limbed symmetric (i.e., single-loop) architectures with serial[3,26,30] or hybrid[7,10] limbs have been proposed, too. Other parallel SMGs are simply obtained by adding a double Cardan shaft (i.e., a limb of RUPUR(1) type),[12,13] which connects the base to the platform, in a translational PM.

Parallel SMGs are faster[6] than their serial counterparts since they allow the possibility of locating the actuators on the base. Nevertheless, reduced workspace and cumbersome multi-loop topologies with complex kinematics are their main drawbacks. In particular, parallel SMGs usually cannot make

* Corresponding author. E-mail: rdigregorio@ing.unife.it
(1)Hereafter, R, P, U and C stand for revolute pair, prismatic pair, universal joint and cylindrical pair, respectively. The underlining indicates the actuated joints and the sequence of joint types, which are encountered by moving from the base to the platform on a limb, is given with a string of capital letters.

the platform perform a complete rotation and some tricks have to be devised for overcoming this drawback.[14] For instance, articulated platforms combined with a rotation amplifier have been used in ref. [6]. This solution exploits a passive not-idle R pair as input either of a gear train or of a toothed belt (rotation amplifier) whose output is another R pair, hinged on the platform, which controls the end effector's rotation.

Also, reducing the number of limbs and keeping the actuators on or near the base is a good compromise to obtain fast machines with a wider workspace. Single-loop architectures with two actuators per limb[3] are a way to satisfy this requirement.

Eventually, not-overconstrained architectures would make it possible to avoid jamming without using small tolerances during manufacturing. Here, a novel parallel SMG of type 2PRPU is studied. Its position analysis, singularity loci and workspace are addressed to provide simple analytic and geometric tools that are useful for the design. The proposed SMG has a single-loop not-overconstrained architecture with actuators on or near the base and make the end effector perform a complete rotation by using a simple rotation amplifier that does not need an articulated platform.

The paper is organized as follows. Section 2 presents the novel parallel SMG together with the adopted notations. Section 3 solves, in closed form, both its direct and inverse position analyses. Then, Section 4 addresses the instantaneous kinematics and identifies its singularity loci, whereas Section 5 studies its dexterous workspace. Eventually, Section 6 discusses a number of issues related to this SMG, and Section 7 draws the conclusions.

2. The 2PRPU: Description and Notations

A single-loop mechanism of type 2PRPU is not-overconstrained and has four-dof. Figure 1 shows a particular 2PRPU mechanism. With reference to Fig. 1, the base and the platform are fixed to the Cartesian references $O_b x_b y_b z_b$ and $O_e x_e y_e z_e$, respectively, and are connected to each other by two PRPU limbs with the PR chain, adjacent to the base, that constitutes a C pair, whose axis is parallel to the axis of the first R pair of the U joint. In addition, the platform is connected to the two limbs by two R pairs (i.e., the second ones of the two U joints) with parallel axes and keeps these axes always parallel during motion. In ref. [3], Lee and Hervé proved that these geometric conditions are sufficient to make the platform perform only Schoenflies motions when singularities do not occur, since this particular 2PRPU mechanism is just a special case of an item in a list of topologies they presented that are suitable to be single-loop SMGs; nevertheless, they did not provide any further analysis on it.

In Fig. 1, one of the axes of the two C pairs is parallel to the x_b axis and the other is parallel to the y_b axis, whereas the axes of the second R pairs of the two U joints are both parallel to the z_b axis. A_1 and A_2 are the centers of the two U joints. B_1 (B_2) is the foot of the perpendicular from A_1 (A_2) to the x_b axis (y_b axis). The directions of the axes of the second R pairs of the two U joints must be parallel to each other and, simultaneously, perpendicular to the axes of the first R pairs of the two U joints, whose directions are fixed by the limb geometry. Thus, the orientations of the planes that contain the two R-pair axes of each U joint do not change during motion.

It is easy to prove, with the screw theory,[15] that each PRPU limb applies to the platform only one torque perpendicular to the plane that contains the two R-pair axes of the U joint. Consequently, the platform of the 2PRPU mechanism of Fig. 1 undergoes only two torques with fixed directions, one parallel to the y_b axis and the other to the x_b axis, which forbid the platform rotations around axes with those two directions. The conclusion is that it can only perform free spatial translations and rotations around axes with the direction of the z_b axis (i.e., Schoenflies motions with rotation axis parallel to the z_b axis).

The parallel SMG presented here is shown in Fig. 2. It is obtained from the 2PRPU mechanism of Fig. 1 by choosing all the P pairs as actuated joints and by adding a rotation amplifier. The rotation amplifier is constituted by a toothed belt that transmits the motion from a pulley, named "fixed pulley" [(2)] in Fig. 2, which is embedded in the hub of the second R pair of the U joint with center at A_1, to another pulley, named "rotating pulley" in Fig. 2, which is embedded in the gripper that, now, is hinged to the platform. Since the hub of the second R pair of the U joint with center at A_1 does not rotate with respect to the base, the "fixed pulley" does not rotate with respect to the base, and its

[(2)]With respect to the base, this pulley translates with the platform without rotating, that is, it keeps a "fixed orientation". The adopted name "fixed pulley" is just an abbreviation of "fixed-orientation pulley".

https://doi.org/10.1017/S0263574718000899 Published online by Cambridge University Press

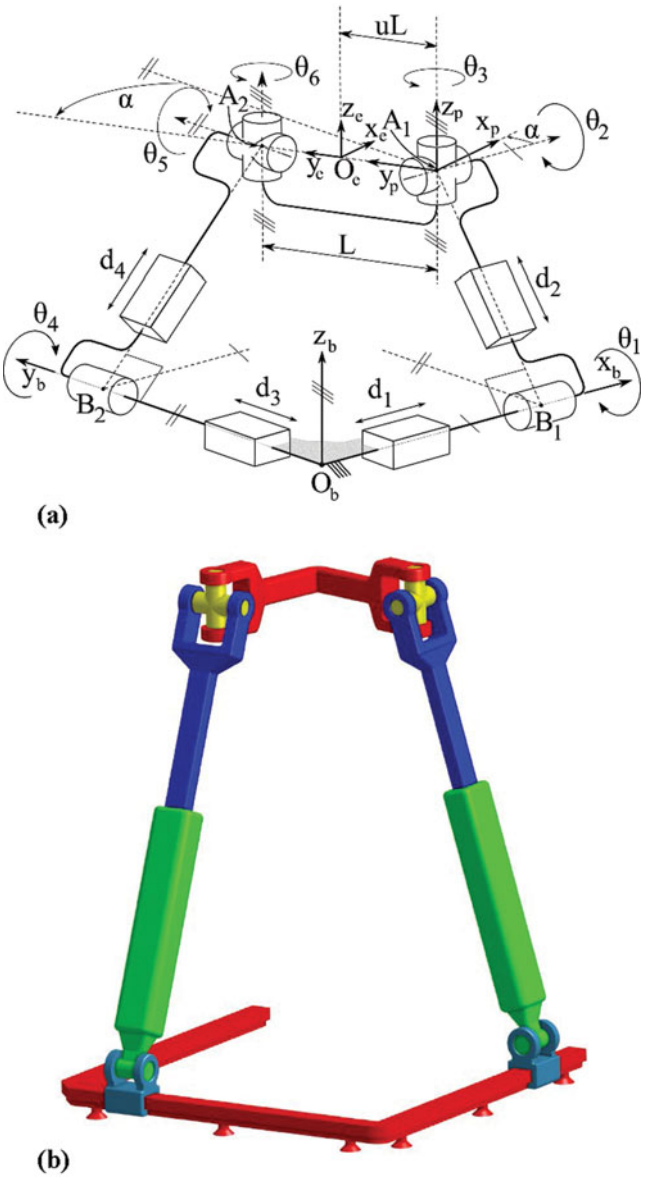

Fig. 1. An SMG of type 2PRPU: (a) Kinematic scheme (parallelepipeds and cylinders denote *P* and *R* pairs, respectively) and (b) 3-D CAD model.

rotation with respect to the platform is equal to the opposite of the platform rotation with respect to the base (i.e., $-\alpha$). Also, the rotation of the "rotating pulley" with respect to the platform has the same direction as the rotation of the "fixed pulley" with respect to the platform. The amplification ratio, k_p, is defined as the ratio between the angular velocities of the gripper and of the platform with respect to the base (i.e., the angular-velocity ratio[16] of this rotation amplifier). As a consequence, k_p is always negative and the angular-velocity ratio of the belt transmission is equal to $(1-k_p)$. Differently from other parallel SMGs that use rotation amplifiers,[14] the proposed solution does not need an articulated platform.

With reference to Figs. 1 and 2, d_1 and d_3 are the signed distances of the points B_1 and B_2, respectively, from O_b and are the joint variables of the two *P* pairs adjacent to the base. d_2 and d_4 are the variable lengths (limb lengths) of the segments B_1A_1 and B_2A_2, respectively, and are the joint variables of the remaining two *P* pairs. L is the constant length of the segment A_1A_2 and u is a constant coefficient ranging from 0 to 1. α is the angle, counterclockwise with respect to the direction of the z_b axis, that the segment A_1A_2 forms with the direction of the y_b axis, and identifies the platform orientation. Eventually, the angles θ_i for $i = 1,\ldots,6$ are the joint variables of the six *R* pairs. θ_1 and

https://doi.org/10.1017/S0263574718000899 Published online by Cambridge University Press

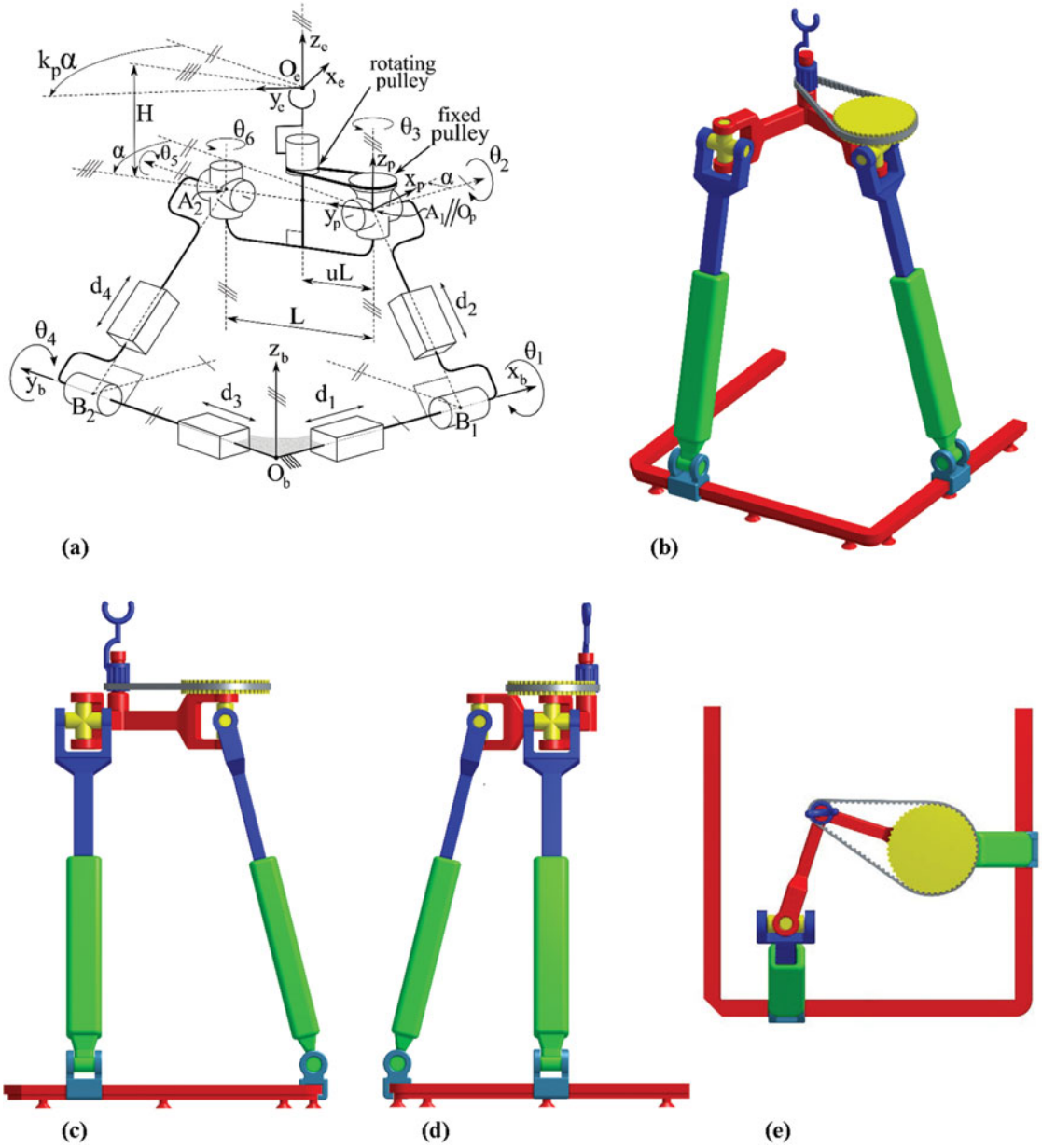

Fig. 2. The SMG of type 2PRPU with rotation amplifier: (a) kinematic scheme and notations, (b) 3-D view of the CAD model, (c) y_bz_b-plane lateral view of the CAD model, (d) x_bz_b-plane lateral view of the CAD model and (e) top view of the CAD model.

θ_2 (θ_4 and θ_5) are defined counterclockwise with respect to the direction of the x_b axis (the y_b axis), whereas θ_3 and θ_6 are defined counterclockwise with respect to the direction of the z_b axis. θ_1 (θ_4) is equal to 0 when the vector ($\boldsymbol{A}_1$–$\boldsymbol{B}_1$) [the vector ($\boldsymbol{A}_2$–$\boldsymbol{B}_2$)] has the same direction of the y_b axis (the x_b axis).

The parallel PM of Fig. 2 has no passive *P* pair. Also, since, in PMs, actuated *P* pairs, which control the limb lengths, are commonly considered near the base enough for not significantly affecting the speed of the PM, the parallel PM of Fig. 2 has two actuators on the base and the remaining two near the base.

3. Position Analysis

The analysis of Fig. 2 reveals that, once the platform pose is determined, the gripper pose is uniquely determined, since the gripper position is obtained by adding the constant vector $(0, 0, H)^T$ to the

https://doi.org/10.1017/S0263574718000899 Published online by Cambridge University Press

coordinates of the platform reference point and the gripper orientation is obtained by amplifying the angle α with the angular-velocity ratio k_p. Hereafter, without losing generality, the mechanism of Fig. 1 will be considered in the kinematic analyses.

With reference to Fig. 1, the four-tuple $\mathbf{q} = (d_1, d_2, d_3, d_4)^T$, which collects all the actuated-joint variables, will be used to locate the points of the joint space. The coordinates $(A_{1x}, A_{1y}, A_{1z})^T$ of the platform point A_1 measured in $O_b x_b y_b z_b$ and the angle α uniquely identify the platform pose, and the four-tuple $\kappa = (A_{1x}, A_{1y}, A_{1z}, \alpha)^T$ will be adopted to locate the points of the operational space.

The inspection of Fig. 1 brings to write the following relationships (bold capital letters denote the position vectors, measured in $O_b x_b y_b z_b$, of the points the letters refer to):

$$\mathbf{B}_1 = \begin{pmatrix} d_1 \\ 0 \\ 0 \end{pmatrix}; \mathbf{B}_2 = \begin{pmatrix} 0 \\ d_3 \\ 0 \end{pmatrix}, \tag{1a}$$

$$\mathbf{A}_1 = \begin{pmatrix} A_{1x} \\ A_{1y} \\ A_{1z} \end{pmatrix} = \begin{pmatrix} d_1 \\ d_2 \cos\theta_1 \\ d_2 \sin\theta_1 \end{pmatrix}; (A_2 - A_1) = \begin{pmatrix} -L\ \sin\alpha \\ L\ \cos\alpha \\ 0 \end{pmatrix}, \tag{1b}$$

$$\mathbf{A}_2 = \begin{pmatrix} A_{2x} \\ A_{2y} \\ A_{2z} \end{pmatrix} = \begin{pmatrix} d_4\ \cos\theta_4 \\ d_3 \\ -d_4\ \sin\theta_4 \end{pmatrix} \equiv \mathbf{A}_1 + (\mathbf{A}_2 - \mathbf{A}_1). \tag{1c}$$

Also, vector Eq. (1c) yields the following closure equations:

$$d_1 - L\ \sin\alpha = d_4 \cos\theta_4, \tag{2a}$$

$$d_3 - L\ \cos\alpha = d_2 \cos\theta_1, \tag{2b}$$

$$d_2\ \sin\theta_1 = -d_4\ \sin\theta_4. \tag{2c}$$

3.1. Inverse position analysis

The inverse position analysis (IPA) consists in the determination of the values of $\mathbf{q}$ compatible with an assigned platform pose (i.e., with an assigned value of κ). In the studied SMG, once A_{1x}, A_{1y}, A_{1z} and α have been assigned, the actuated-joint variables d_1 and d_2 can be immediately computed as follows (see Eqs. (1a) and (1b)):

$$d_1 = A_{1x}; \quad d_2 = |\mathbf{A}_1 - \mathbf{B}_1| = \sqrt{A_{1y}^2 + A_{1z}^2}. \tag{3}$$

Then, the coordinates of point A_2 can be computed with the last of formulas (1c) that yields

$$A_{2x} = A_{1x} - L\ \sin\alpha; \quad A_{2y} = A_{1y} + L\ \cos\alpha; \quad A_{2z} = A_{1z}. \tag{4}$$

Eventually, the remaining actuated-joint variables, d_3 and d_4, can be computed with the following formulas:

$$d_3 = A_{2y}; \quad d_4 = |\mathbf{A}_2 - \mathbf{B}_2| = \sqrt{A_{2x}^2 + A_{2z}^2}. \tag{5}$$

The conclusion is that the IPA has only one solution computable with simple explicit formulas.

https://doi.org/10.1017/S0263574718000899 Published online by Cambridge University Press

3.2. Direct position analysis

The direct position analysis (DPA) consists in the determination of the platform poses (i.e., of the values of κ) compatible with assigned actuated-joint variables (i.e., with an assigned value of $\mathbf{q}$). In the studied SMG, if the coordinates of points A_1 and A_2 are computed as a function of the actuated-joint variables, d_i for $i = 1,\ldots,4$, the platform pose will be known as a function of the same variables and the angle α can be computed with the second of formulas (1b) thus solving the DPA. Regarding these coordinates, Eqs. (3)–(5) highlight that A_{1x} and A_{2y} are immediately expressible as a function of the actuated-joint variables, whereas A_{2z} is equal to A_{1z}. Therefore, only the coordinates A_{1y}, A_{1z} and A_{2x} must be computed to solve the DPA. This computation is reported below.

The following three scalar equations can be written (see Fig. 1):

$$(\mathbf{A}_2 - \mathbf{A}_1) \cdot (\mathbf{A}_2 - \mathbf{A}_1) = L^2, \tag{6a}$$

$$(\mathbf{A}_1 - \mathbf{B}_1) \cdot (\mathbf{A}_1 - \mathbf{B}_1) = {d_2}^2, \tag{6b}$$

$$(\mathbf{A}_2 - \mathbf{B}_2) \cdot (\mathbf{A}_2 - \mathbf{B}_2) = {d_4}^2, \tag{6c}$$

which by taking into account Eqs. (1), (3), (4) and (5) become

$$(A_{2x} - d_1)^2 + (d_3 - A_{1y})^2 = L^2, \tag{7a}$$

$${A_{1y}}^2 + {A_{1z}}^2 = {d_2}^2, \tag{7b}$$

$${A_{2x}}^2 + {A_{1z}}^2 = {d_4}^2. \tag{7c}$$

Equations (7a)–(7c) constitute a non-linear system of three equations in the three unknowns A_{1y}, A_{1z} and A_{2x}. System (7) can be further reduced by linearly eliminating A_{1z}^2 in Eqs. (7b) and (7c). So doing, it becomes (the left-hand side of Eq. (7a) has been expanded)

$${A_{2x}}^2 + {A_{1y}}^2 - 2d_1\, A_{2x} - 2d_3 A_{1y} + {d_1}^2 + {d_3}^2 = L^2, \tag{8a}$$

$${A_{2x}}^2 - {A_{1y}}^2 = {d_4}^2 - {d_2}^2. \tag{8b}$$

The sum of Eqs. (8a) and (8b) yields

$$A_{1y} = b_2 {A_{2x}}^2 + b_1 A_{2x} + b_0, \tag{9}$$

where $b_0 = (d_1^2 + d_2^2 + d_3^2 - d_4^2 - L^2)/2d_3$, $b_1 = -d_1/d_3$, and $b_2 = 1/d_3$.

The introduction of expression (9) into Eq. (8b) gives the following univariate polynomial equation of degree 4 in A_{2x}:

$${A_{2x}}^2 - (b_2 {A_{2x}}^2 + b_1 A_{2x} + b_0)^2 = {d_4}^2 - {d_2}^2, \tag{10}$$

which can be solved in closed form[17] and gives four complex (i.e., up to four real) values of A_{2x}. The computed values of A_{2x}, when back substituted into Eqs. (9) and (7c), yield as many values of A_{1y} and two opposite values of A_{1z} for each A_{2x} given by the formula

$$A_{1z} = \pm\sqrt{d_4^2 - A_{2x}^2}. \tag{11}$$

https://doi.org/10.1017/S0263574718000899 Published online by Cambridge University Press

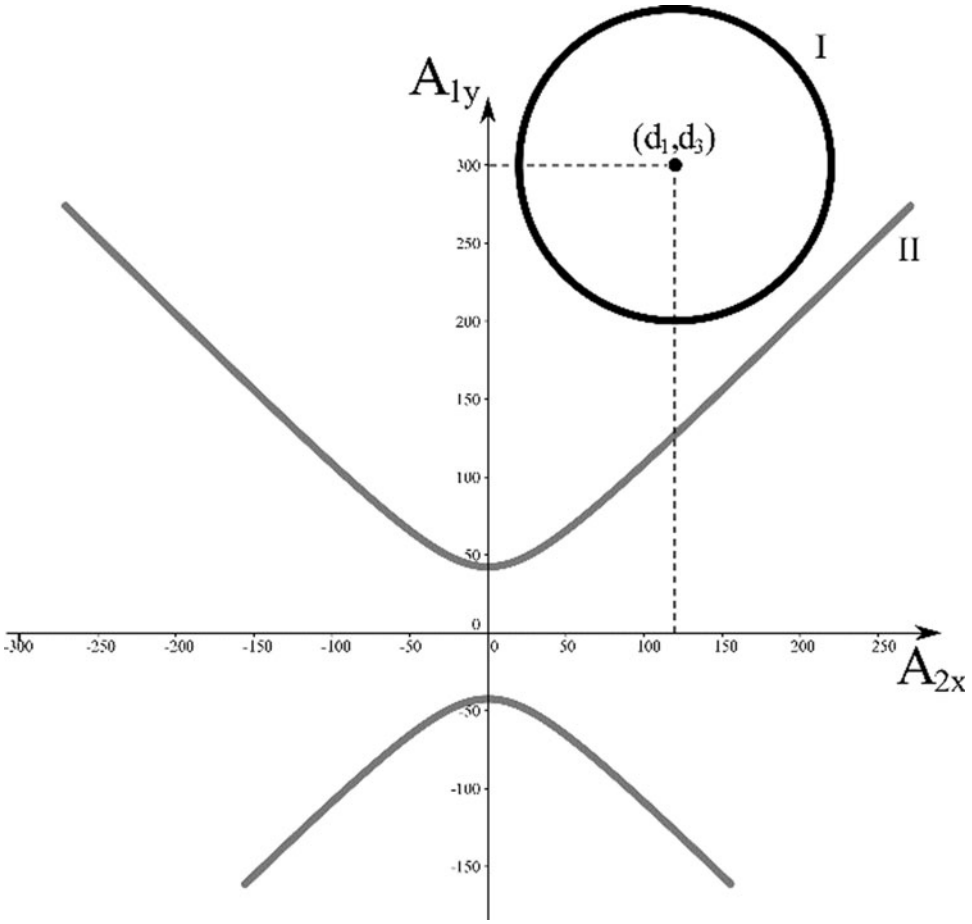

Fig. 3. No real DPA solution ($d_1 = 120$ l.u., $d_2 = 450$ l.u., $d_3 = 300$ l.u., $d_4 = 448$ l.u., $L = 100$ l.u.; l.u. stands for a generic "length unit").

The conclusion is that the DPA has up to eight solutions symmetrically disposed with respect to the plane x_by_b, which can be computed in closed form.

From a geometric point of view, in a Cartesian plane with A_{2x} and A_{1y} as abscissa and ordinate, respectively, Eq. (8a) [Eq. (7a)] is a circumference with center at (d_1, d_3) and radius L, whereas Eq. (8b) is a rectangular hyperbola with the two lines $A_{1y} = \pm A_{2x}$ as asymptotes. Thus, the real solutions of system (8) are the possible intersections of these two curves. Figs. 3–5 show three cases: the first with no real solution, the second with only two real solutions and the third with four real solutions. Such diagrams are useful tools for visualizing the effects of the values of the actuated-joint variables on the DPA since changing (d_1, d_3) corresponds to rigidly translating the circumference, whereas the variation of $(d_4^2–d_2^2)$ modifies the hyperbola without affecting its asymptotes (i.e., only the central part of the hyperbola is modified in practice). Also, since each real solution of system (8) corresponds to two real DPA solutions, which are symmetrically located with respect to the coordinate plane x_by_b, they show that eight real DPA solutions may actually occur.

4. Instantaneous Kinematics

The determination and the analysis of the linear relationship between the actuated-joint rates (instantaneous inputs) and the platform twist (instantaneous output) are the subjects of the instantaneous kinematics. Such a relationship is named the instantaneous input–output relationship (InI/O). In the studied SMG, $\dot{\mathbf{q}} = (\dot{d}_1, \dot{d}_2, \dot{d}_3, \dot{d}_4)^T$ is the four-tuple that collects the actuated-joint rates, whereas the platform twist can be identified by $\dot{\kappa} = (\dot{A}_{1x}, \dot{A}_{1y}, \dot{A}_{1z}, \dot{\alpha})$ only if manipulator configurations (constraint singularities[18]) where the platform motion can instantaneously be different from a Schoenflies motion are not present.

https://doi.org/10.1017/S0263574718000899 Published online by Cambridge University Press

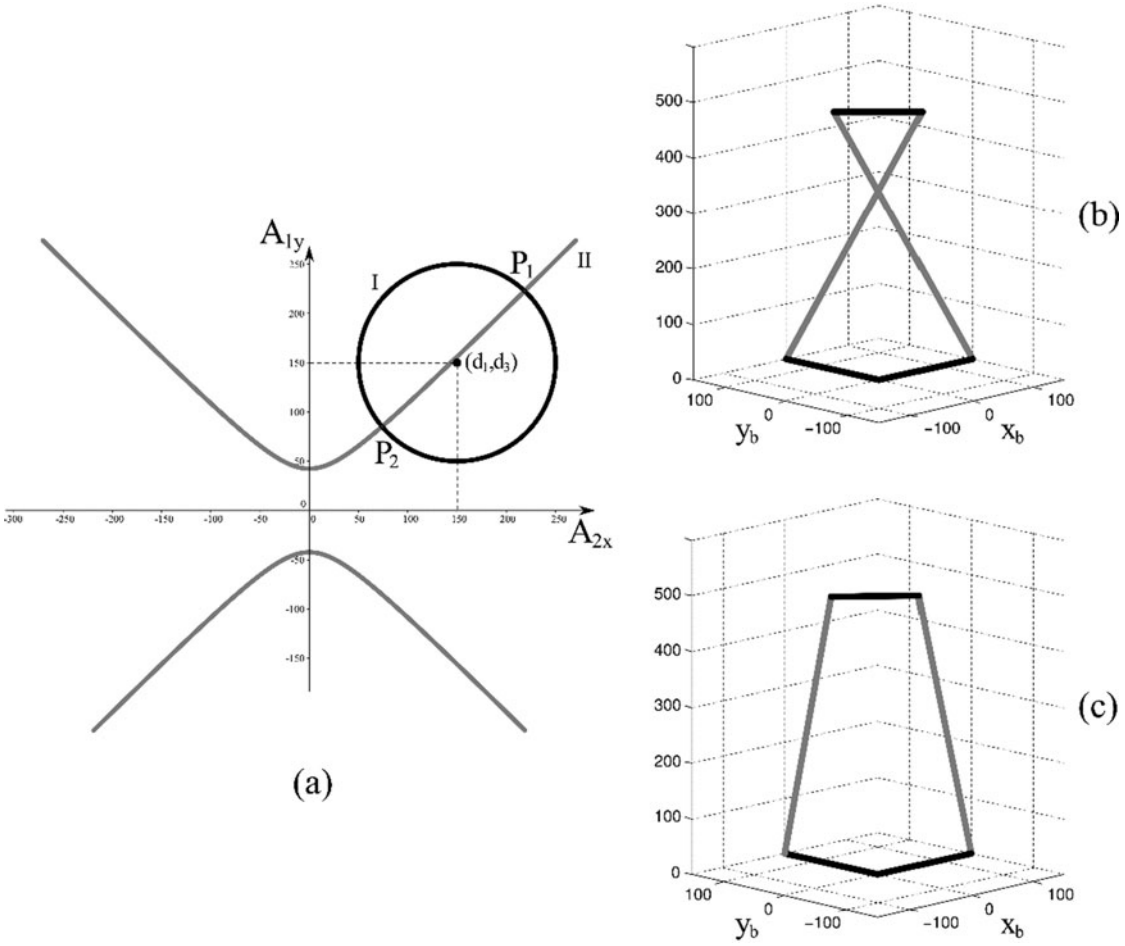

Fig. 4. Two real solutions of system (8) corresponding to four real DPA solutions symmetrically disposed with respect to the plane x_by_b ($d_1 = 150$ l.u., $d_2 = 450$ l.u., $d_3 = 150$ l.u., $d_4 = 448$ l.u., $L = 100$ l.u.; l.u. stands for a generic "length unit"): (a) graphical solution of system (8), (b) manipulator configuration, located in the region $z_b > 0$, which corresponds to the solution P_1 (i.e., $A_{2x} = 218.65$ l.u., $A_{1y} = 222.72$ l.u.) and (c) manipulator configuration, located in the region $z_b > 0$, which corresponds to the solution P_2 (i.e., $A_{2x} = 73.87$ l.u., $A_{1y} = 85.16$ l.u.).

With reference to Fig. 1, the fact that the two ending R pairs of the two limbs must be parallel to one another from the platform's geometry and, at the same time, one R pair must be perpendicular to the x_b axis and the other to the y_b axis from the limbs' geometry, constrains their axes to be always parallel to the z_b axis. As a consequence, the angular velocity, ω, of the platform can be written in the following two different ways according to the limb used to compute it ($\mathbf{i}_b$, $\mathbf{j}_b$ and $\mathbf{k}_b$ are the unit vectors of the axes x_b, y_b and z_b, respectively)

$$\omega = (\dot{\theta}_1 + \dot{\theta}_2)\mathbf{i}_b + \dot{\theta}_3\mathbf{k}_b, \tag{12a}$$

$$\omega = (\dot{\theta}_4 + \dot{\theta}_5)\mathbf{j}_b + \dot{\theta}_6\mathbf{k}_b. \tag{12b}$$

Equating the right-hand sides of Eqs. (12a) and (12b) yields

$$(\dot{\theta}_1 + \dot{\theta}_2)\mathbf{i}_b - (\dot{\theta}_4 + \dot{\theta}_5)\mathbf{j}_b + (\dot{\theta}_3 - \dot{\theta}_6)\mathbf{k}_b = 0. \tag{13}$$

Equation (13) can be satisfied if and only if the coefficients of the three independent unit vectors $\mathbf{i}_b$, $\mathbf{j}_b$ and $\mathbf{k}_b$ are identically equal to zero. Since the coefficients of $\mathbf{i}_b$ and $\mathbf{j}_b$ are the same that appear in the first terms at the right-hand sides of Eqs. (12a) and (12b), the platform angular velocity must

https://doi.org/10.1017/S0263574718000899 Published online by Cambridge University Press

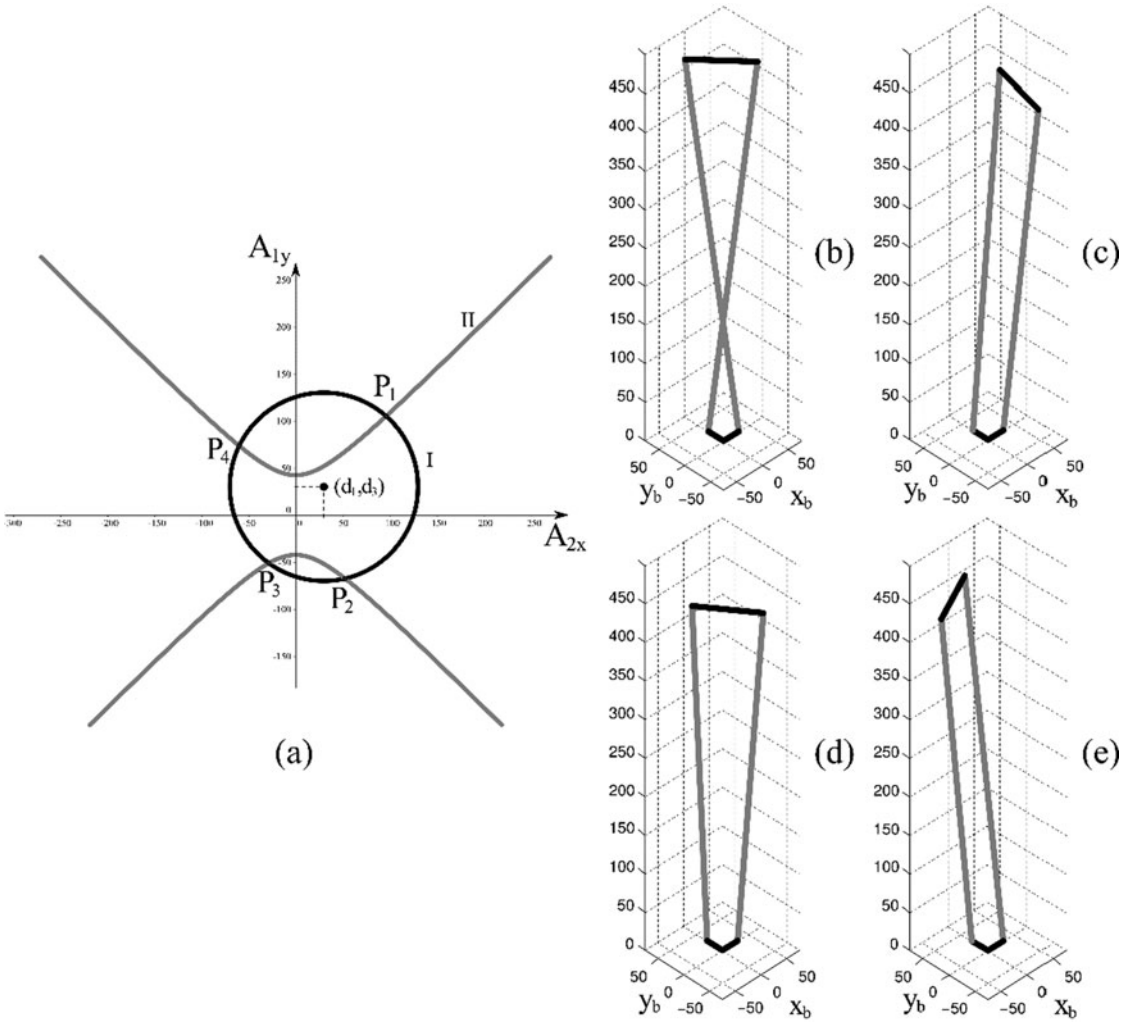

Fig. 5. Four real solutions of system (8) corresponding to eight real DPA solutions symmetrically disposed with respect to the plane x_by_b ($d_1 = 30$ l.u., $d_2 = 450$ l.u., $d_3 = 30$ l.u., $d_4 = 448$ l.u., $L = 100$ l.u.; l.u. stands for a generic "length unit"): (a) graphical solution of system (8), (b) manipulator configuration, located in the region $z_b > 0$, which corresponds to the solution P_1 (i.e., $A_{2x} = 96.11$ l.u., $A_{1y} = 105.03$ l.u.), (c) manipulator configuration, located in the region $z_b > 0$, which corresponds to the solution P_2 (i.e., $A_{2x} = 52.47$ l.u., $A_{1y} = -67.44$ l.u.), (d) manipulator configuration, located in the region $z_b > 0$, which corresponds to the solution P_3 (i.e., $A_{2x} = -28.53$ l.u., $A_{1y} = -51.09$ l.u.), and (e) manipulator configuration, located in the region $z_b > 0$, which corresponds to the solution P_4 (i.e., $A_{2x} = -60.05$ l.u., $A_{1y} = 73.49$ l.u.).

always be parallel to $\mathbf{k}_b$. Thus, the occurrence of constraint singularities is excluded and the platform twist can be identified by $\dot{\kappa} = (\dot{A}_{1x}, \dot{A}_{1y}, \dot{A}_{1z}, \dot{\alpha})$.

In order to deduce the InI/O, the following four constraint equations can be selected/deduced from Equations (3)–(5), (7b) and (7c):

$$A_{1x} = d_1, \tag{14a}$$

$$A_{1y}{}^2 + A_{1z}{}^2 = d_2{}^2, \tag{14b}$$

$$A_{1y} + L\cos\alpha = d_3, \tag{14c}$$

$$(A_{1x} - L\sin\alpha)^2 + A_{1z}{}^2 = d_4{}^2, \tag{14d}$$

whose time derivatives yield the following InI/O:

$$\mathbf{M}\,\dot{\kappa} = \mathbf{N}\,\dot{\mathbf{q}}, \tag{15}$$

https://doi.org/10.1017/S0263574718000899 Published online by Cambridge University Press

where the Jacobian matrices **M** and **N** are defined as follows:

$$\mathbf{M} = \begin{bmatrix} 1 & 0 & 0 & 0 \\ 0 & A_{1y} & A_{1z} & 0 \\ 0 & 1 & 0 & -L\sin\alpha \\ A_{1x} - L\sin\alpha & 0 & A_{1z} & L\cos\alpha(L\sin\alpha - A_{1x}) \end{bmatrix}, \tag{16a}$$

$$N = \begin{bmatrix} 1 & 0 & 0 & 0 \\ 0 & d_2 & 0 & 0 \\ 0 & 0 & 1 & 0 \\ 0 & 0 & 0 & d_4 \end{bmatrix}. \tag{16b}$$

4.1. Singularity analysis

Singular configurations (singularities) are manipulator configurations where the InI/O fails to state a one-to-one correspondence between actuated-joint rates and platform twists.[18–21] The InI/O allows the solution of two problems relevant in the control of a manipulator[21]: (i) the determination of the actuated-joint rates for an assigned platform twist [Instantaneous Inverse Kinematic Problem (IIKP)] and (ii) the determination of the platform twist for assigned actuated-joint rates [Instantaneous Forward Kinematic Problem (IFKP)]. The solution of these problems depends on the manipulator configuration since the Jacobian matrices appearing in the InI/O depend on it. In ref. [19], singularities have been collected into three types according to which of these problems is undetermined: (i) the IIKP is undetermined, (ii) the IFKP is undetermined and (iii) both IIKP and IFKP are undetermined. Then, in ref. [21], this classification has been further detailed by taking into account the passive-joint variables.

Singularities play an important role in the static behavior of a manipulator and must be determined during its design. In particular, type-I singularities are located at the workspace boundaries and correspond to configurations where the platform can carry external loads without requiring that generalized torques are applied by one or more actuators. Also, type-II singularities can be located inside the workspace and correspond to configurations where infinite generalized torques must be applied by at least one actuator to make the platform carry external loads (even infinitesimal).

In the studied SMG, the above-deduced InI/O (i.e., system (15)) shows that type-I singularities occur when det(**N**) is equal to zero, type-II singularities occur when det(**M**) is equal to zero, and type-III singularities occur when det(**M**) and det(**N**) are both equal to zero. The analytic expressions of these two determinants are [see Eqs. (16a) and (16b)]

$$\det(\mathbf{M}) = LA_{1z}[A_{1y}\sin\alpha + \cos\alpha(A_{1x} - L\sin\alpha)] \equiv LA_{1z}[A_{1y}\sin\alpha + \cos\alpha A_{2x}], \tag{17a}$$

$$\det(\mathbf{N}) = d_2 d_4. \tag{17b}$$

Therefore, type-I singularities occur when either d_2 or d_4 are equal to zero, both these conditions cannot be reached in practice for the actual physical dimensions of the limbs. Type-II singularities occur when either of the following conditions are satisfied:

$$A_{1z} = 0, \tag{18a}$$

$$A_{1y}\sin\alpha + A_{2x}\cos\alpha = 0. \tag{18b}$$

Condition (18a) corresponds to a configuration where the manipulator is flattened on the $x_b y_b$ plane (see Fig. 1). It is worth noting that, if this condition is satisfied, the third column of matrix **M** will be a null vector and $\dot{A}_{1z}$ cannot be computed with the actuated-joint rates any longer. From a kinematic point of view, the indeterminacy of $\dot{A}_{1z}$ means that the actuators are not able to control the platform translation along the z_b axis when this flattened configuration is reached.

https://doi.org/10.1017/S0263574718000899 Published online by Cambridge University Press

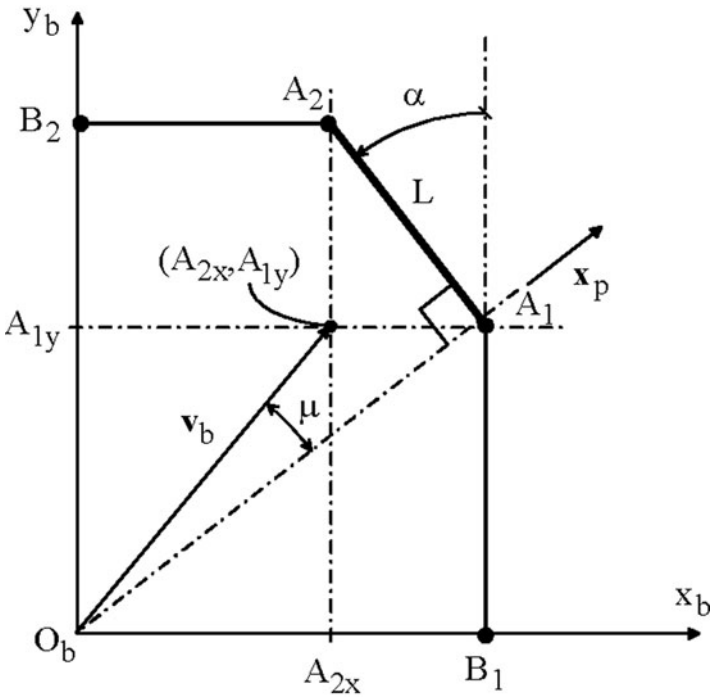

Fig. 6. Projection of a generic configuration of the 2PRPU SMG onto the x_by_b plane together with the vectors $\mathbf{v}_b$ and $\mathbf{x}_p$: singularity condition (18b) is satisfied when $|\mu| = 90^\circ$.

Condition (18b) is more difficult to interpret. The analytic solution of system (15) obtained by transforming matrix $\mathbf{M}$ into an upper triangular matrix with the Gaussian elimination[22] highlights that the left-hand side of Eq. (18b) is the coefficient of $\dot{\alpha}$ in the last row of the triangular matrix. Therefore, when this coefficient is equal to zero, $\dot{\alpha}$ cannot be computed with the actuated-joint rates any longer, and the actuators are not able to control the platform orientation. From a geometric point of view (Fig. 6), such coefficient can be interpreted as the dot product, $\mathbf{v}_b \cdot \mathbf{x}_p$, of two planar vectors: $\mathbf{v}_b = (A_{2x}, A_{1y})^T$ and $\mathbf{x}_p = (\cos\,\alpha,\, \sin\,\alpha)^T$, which is a unit vector perpendicular to the projection onto the x_by_b plane of the vector $(\boldsymbol{A}_2\text{–}\boldsymbol{A}_1)$ [see Eq. (1b)]. The manipulator configurations where these two vectors are perpendicular make the coefficient equal to zero and the platform orientation out of control. The perpendicularity of $\mathbf{v}_b$ and $\mathbf{x}_p$ corresponds to the parallelism of $\mathbf{v}_b$ and $(\mathbf{A}_2\text{–}\mathbf{A}_1)$. Also, condition (18b) can be rewritten in the following form:

$$\tan\alpha = -\frac{A_{2x}}{A_{1y}}, \tag{19}$$

which highlights that—for $\alpha \in [0^\circ, 90^\circ]$, if the projections of A_1 and A_2 (Fig. 6) lie on either the first or the third quadrant of the x_by_b plane (i.e., when $A_{1y}A_{2x} \geq 0$) condition (18b) is satisfied only when the manipulator is flattened either on the y_bz_b plane ($\alpha = 0^\circ$ and $A_{2x} = 0$) or on the x_bz_b plane ($\alpha = 90^\circ$ and $A_{1y} = 0$)—for $\alpha \in [-90^\circ, 0^\circ]$, if the projections of A_1 and A_2 (Fig. 6) lie on either the second or the fourth quadrant of the x_by_b plane (i.e., when $A_{1y}A_{2x} \leq 0$) condition (18b) is satisfied only when the manipulator is flattened either on the y_bz_b plane ($\alpha = 0^\circ$ and $A_{2x} = 0$) or on the x_bz_b plane ($\alpha = -90^\circ$ and $A_{1y} = 0$).

The conclusion is that, if the limitations $0^\circ < |\alpha| < 90^\circ$ and $|A_{1z}| > 0$ are introduced, there are always two separate octants of the Cartesian reference $O_bx_by_bz_b$, whose location depends on the chosen signs of α and A_{1z}, where the platform can be moved without encountering type-II singularities. In each of these octants, even though the platform rotation is limited, the gripper rotation (Fig. 2) can be a complete rotation by choosing a suitable value of the angular-velocity ratio k_p of the rotation amplifier.

https://doi.org/10.1017/S0263574718000899 Published online by Cambridge University Press

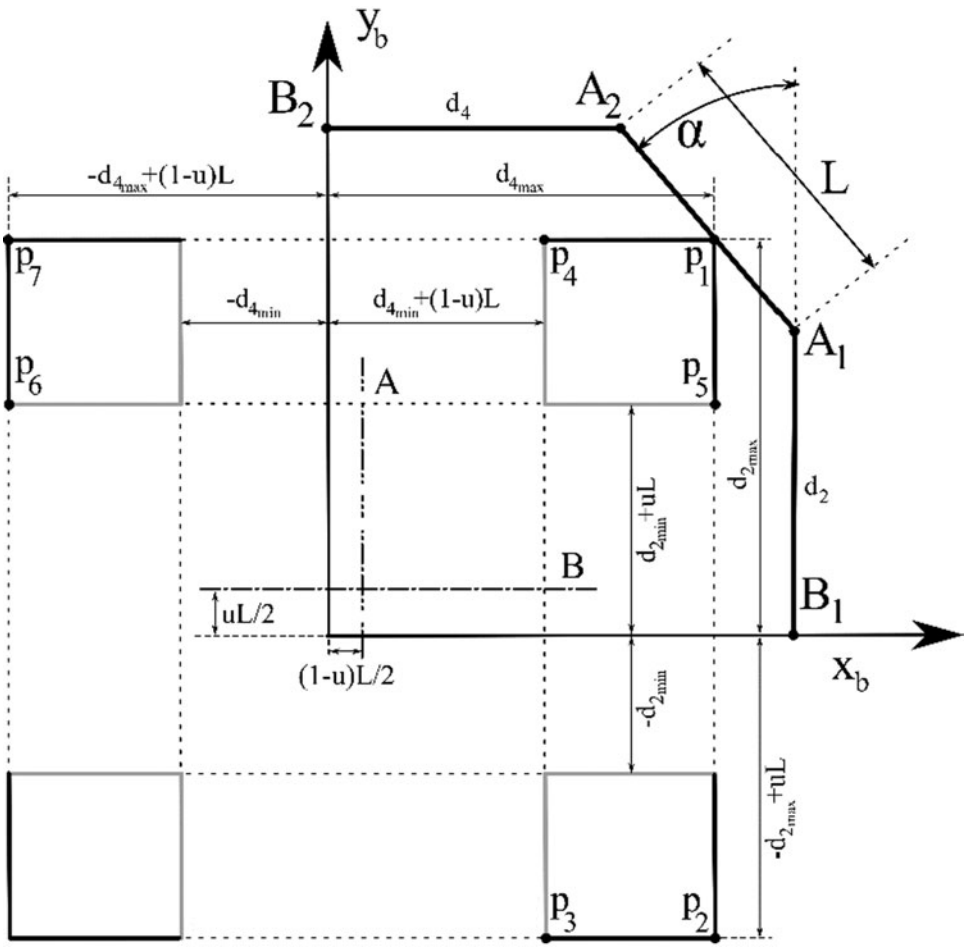

Fig. 7. Dexterous workspace of the 2PRPU SMG sectioned with the x_by_b plane: the points p_i, for $i = 1,\ldots,7$, are the reference vertices of the four rectangles that constitute this section.

5. Workspace Analysis

Since the position of the gripper's reference point O_e (see Fig. 2) is obtained from the position of the homonymous platform point of Fig. 1 by adding the constant translation $(0, 0, H)^T$, and the rotation range of the gripper is the product of the platform rotation range by the angular-velocity ratio k_p of the rotation amplifier, for the sake of clarity and without losing generality, this workspace analysis will be referred to the platform and to the notations of Fig. 1.

The shape of the dexterous workspace [23] depends on the ranges[(3)] chosen for α, d_1, d_2, d_3 and d_4, and on the values of the geometric constants u and L. Hereafter, the dexterous workspace will be represented by giving the positions that the platform point O_e (Fig. 1) can reach with any platform orientation in the range $0^\circ \leq \alpha \leq 90^\circ$. Such workspace is the intersection of two right circular cylindrical shells due to the two PRPU limbs (see Figs. 7 and 8). One shell has the axis (axis B in Fig. 7) parallel to the x_b axis and passing through the point $\{(1–u)L/2, uL/2, 0\}^T$, and the inner and outer radii equal to $(d_{2min}+uL/2)$ and $(d_{2max} - uL/2)$, respectively (i.e., with reference to Fig. 7, the shell obtained by rotating around the axis B the rectangle whose vertices are the points p_1, p_5, p_6 and p_7). The other shell has the axis (axis A in Fig. 7) parallel to the y_b axis and passing through the point $\{(1–u)L/2, uL/2, 0\}^T$, and the inner and outer radii equal to $[d_{4min}+(1–u)L/2]$ and $[d_{4max}–(1–u)L/2]$, respectively (i.e., with reference to Fig. 7, the shell obtained by rotating around the axis A the rectangle whose vertices are the points p_1, p_2, p_3 and p_4). The section of this workspace with the x_by_b plane consists of four rectangles symmetrically located with respect to the axes of the two right circular

[(3)]Hereafter, the minimum and the maximum values of α, d_1, d_2, d_3 and d_4 will be denoted with the right subscripts "min" and "max", respectively, added to the symbols of the variables.

https://doi.org/10.1017/S0263574718000899 Published online by Cambridge University Press

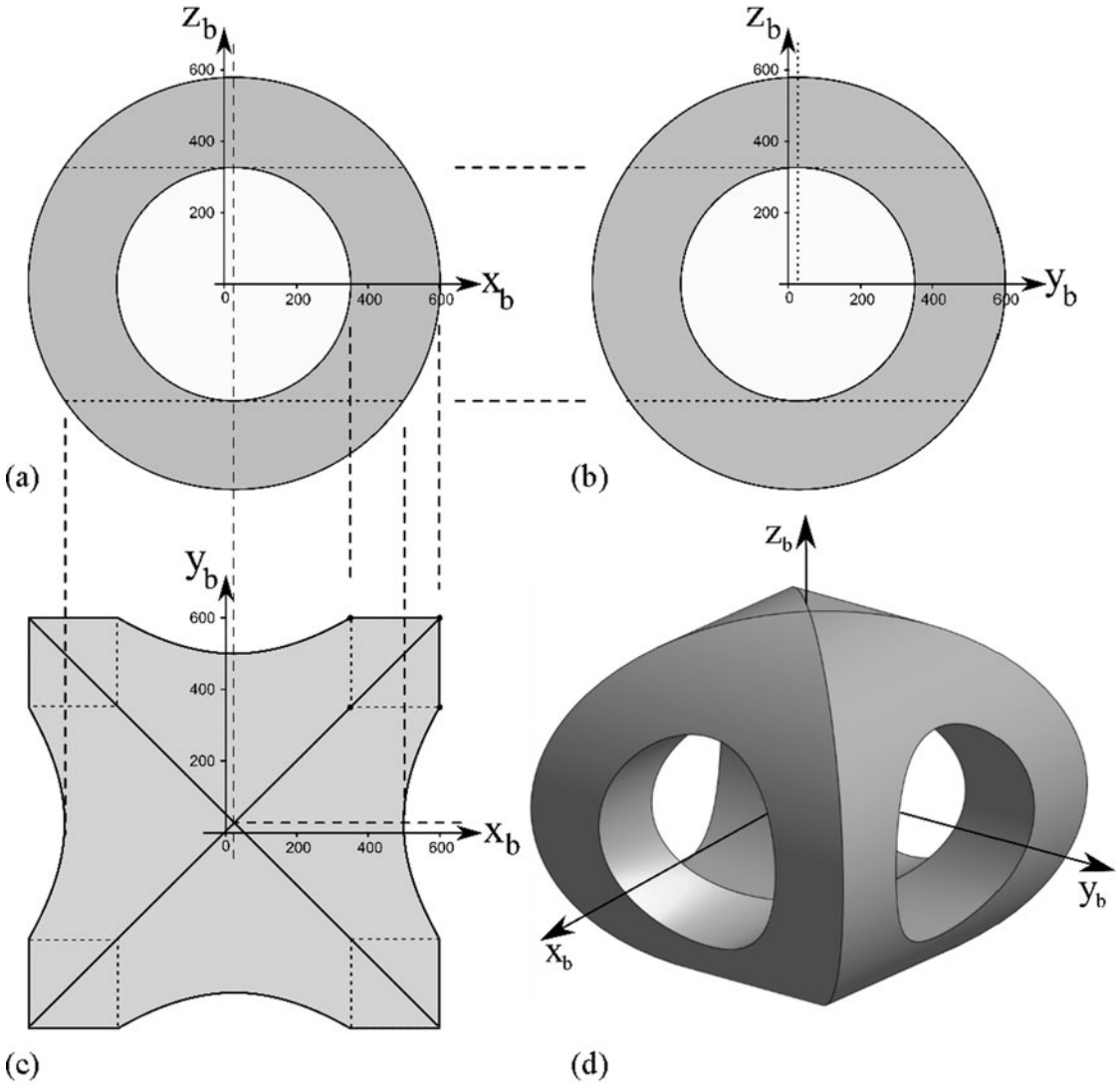

Fig. 8. Dexterous workspace for $u = 0.5$, $L = 100$ l.u., $d_{2min} = d_{4min} = 3$ L and $d_{2max} = d_{4max} = 6$ L: (a) $x_b z_b$ section, (b) $y_b z_b$ section, (c) $x_b y_b$ section and (d) 3-D view.

cylindrical shells. Figure 7 shows this section together with a manipulator configuration located at the workspace boundary,[4] whereas Fig. 8 shows the 3-D diagram of the dexterous workspace for $u = 0.5$, $L = 100$ l.u., $d_{2min} = d_{4min} = 3$ L and $d_{2max} = d_{4max} = 6$ L.

Since, as proved in the previous section, singularity conditions are not encountered when the segment A_1A_2 is in the first octant of the Cartesian reference $O_b x_b y_b z_b$, and Eq. (2) relates d_1 and d_3 to d_2 and d_4, in order to determine a free-from-singularities (FFS) dexterous workspace, the minimum and the maximum values of d_1 and d_3 can be computed as follows (see Fig. 7):

$$d_{1\min} = (1-u)L, \quad d_{1\max} = d_{4\max} + uL, \quad d_{3\min} = uL, \quad d_{3\max} = d_{2\max} + (1-u)L. \tag{20}$$

Figure 9 shows how this FFS dexterous workspace changes for three different values of u, namely, $u = 0.2$, $u = 0.5$ and $u = 0.8$, whereas Fig. 10 shows how the volume, V, of this workspace changes as a function of u and that the maximum value of V corresponds to $u = 0.5$.

By keeping $u = 0.5$, $d_{2min} = d_{4min} = 3$L and $d_{2max} = d_{4max}$, the dimensionless volume, V/L^3, of the FFS dexterous workspace depends only on the ratios d_{2max}/d_{2min} since the ranges of the other

[4]The manipulator configuration shown in Fig. 7 refers to a manipulator with $u = 0.5$.

https://doi.org/10.1017/S0263574718000899 Published online by Cambridge University Press

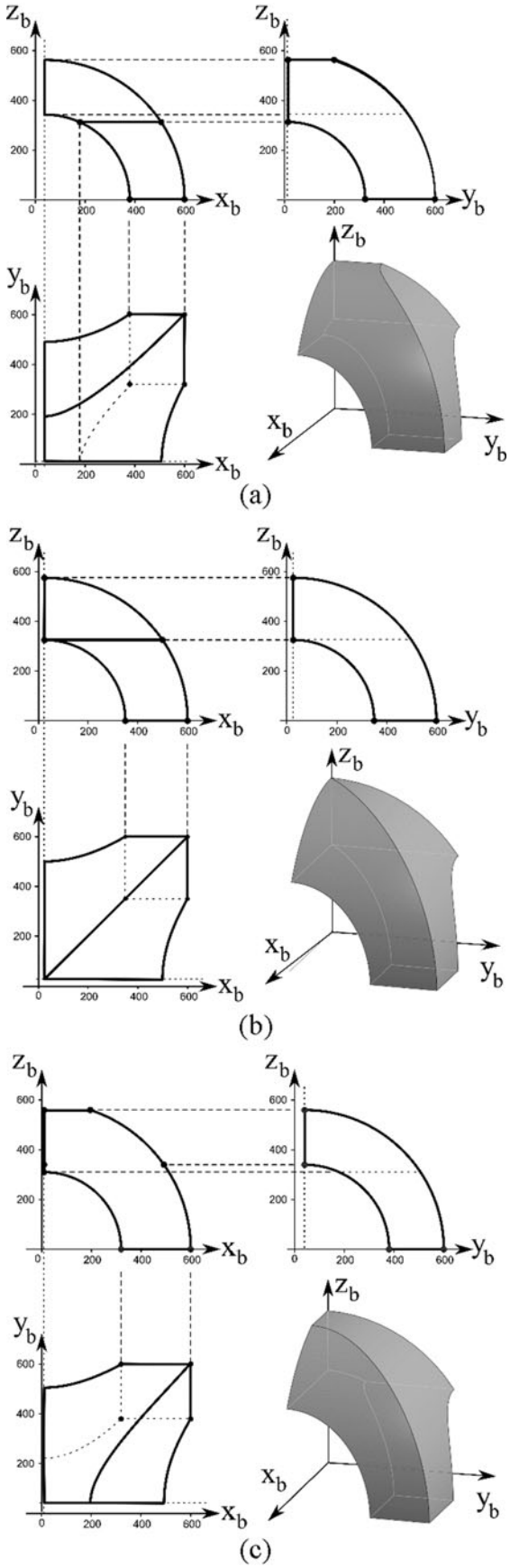

Fig. 9. Free-from-singularities dexterous workspace ($L = 100$ l.u., $d_{2min} = d_{4min} = 3$ L and $d_{2max} = d_{4max} = 6$ L) for (a) $u = 0.2$, (b) $u = 0.5$, and (c) $u = 0.8$.

https://doi.org/10.1017/S0263574718000899 Published online by Cambridge University Press

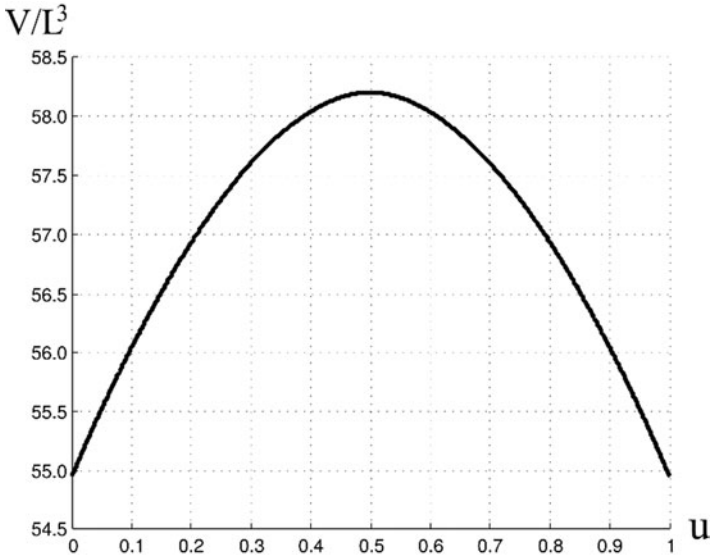

Fig. 10. Dimensionless volume, V/L^3, of the free-from-singularities dexterous workspace as a function of the parameter u for $d_{2min} = d_{4min} = 3$ L and $d_{2max} = d_{4max} = 6$ L.

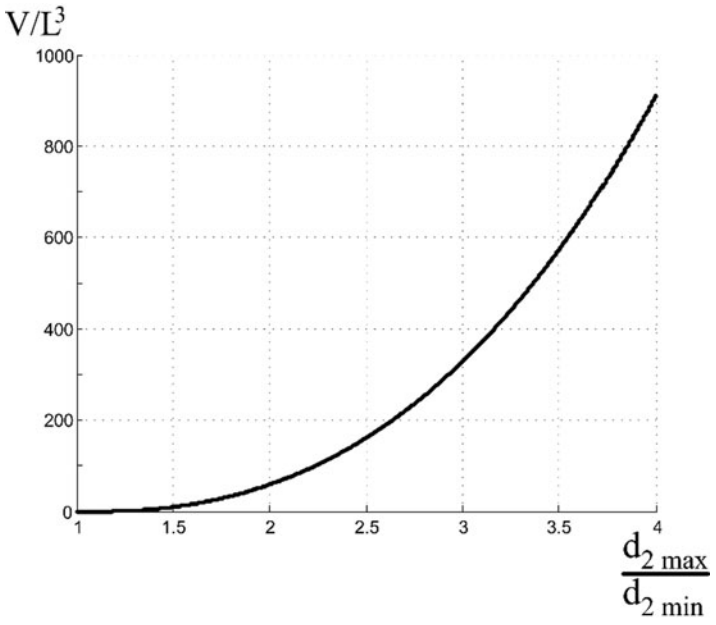

Fig. 11. Dimensionless volume, V/L^3, of the free-from-singularities dexterous workspace as a function of the d_{2max}/d_{2min} for $u = 0.5$, $(d_{2min}/\mathrm{L}) = (d_{4min}/\mathrm{L}) = 3$ and $d_{2max} = d_{4max}$.

dimensionless variables, d_1/L and d_3/L, can be computed through Eq. (20). Figure 11 shows the diagram of V/L^3 as a function of d_{2max}/d_{2min} for $u = 0.5$, $d_{2min} = d_{4min} = 3$L and $d_{2max} = d_{4max}$. The analysis of Fig. 11 highlights that the volume of the FFS dexterous workspace increases more than six times passing from $(d_{2max}/d_{2min}) = 2$, which is the value of Fig. 9(b), to (d_{2max}/d_{2min})=3. Figure 12 shows the FFS dexterous workspace for $(d_{2max}/d_{2min}) = 3$, $u = 0.5$, $L = 100$ l.u., $d_{2min} = d_{4min} = 3L$ and $d_{2max} = d_{4max}$. The analysis of Fig. 12 reveals that the FFS dexterous workspace is wide enough for including useful workspace suitable for real applications.

https://doi.org/10.1017/S0263574718000899 Published online by Cambridge University Press

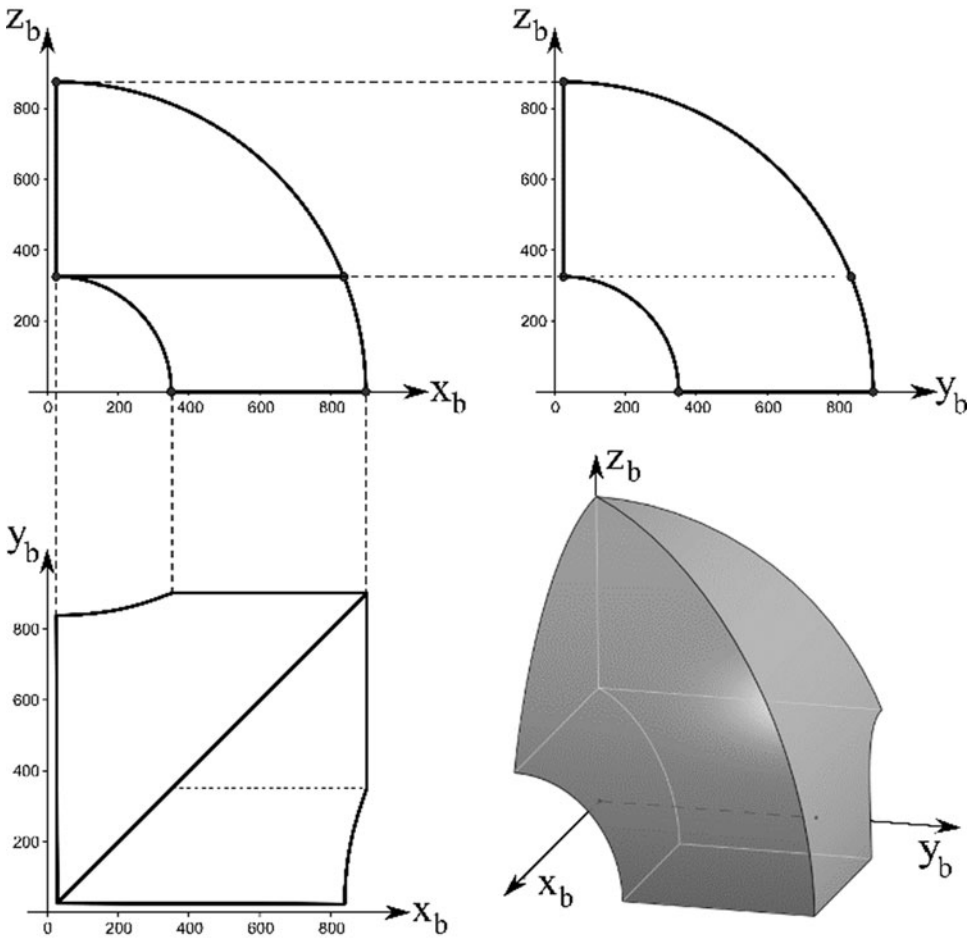

Fig. 12. Free-from-singularities dexterous workspace for $(d_{2max}/d_{2min}) = 3, u = 0.5, L = 100$ l.u., $d_{2min} = d_{4min} =$ 3 L and $d_{2max} = d_{4max}$.

6. Discussion

This section provides pieces of information on stiffness, performance analysis and optimal design of the proposed SMG.

Regarding the stiffness of the proposed SMG, the usual stiffness analyses (see, for instance, refs. [24, 25]) keep the links rigid and concentrate flexibility in the actuated joints. In addition, the same analyses reduce the stiffness matrix of the actuated joints to a stiffness coefficient that multiplies an identity matrix and bring to conclude that the stiffer configurations are the ones that are far from type-II singularities. In the case under study, since all the actuated joints are *P* pairs, the hypothesis that they all have the same stiffness coefficient is applicable and brings to a stiffness matrix of the actuated joints equal to a stiffness coefficient that multiplies the 4x4 identity matrix. Therefore, the presented singularity analysis also provide information on the stiffness of the manipulator, which also depends on the stiffness coefficient of the chosen actuated *P* pairs. According to this conclusion, its payload capability is related to the stiffness coefficient of the chosen actuated *P* pairs. Since the majority of PMs adopt actuated *P* pairs, the limitation on the payload capability due to the stiffness is comparable to the one of other PMs.

Regarding the performance analysis and the optimal design, the following subsection addresses the performance analysis based on kinetostatics and the optimal design of the proposed SMG.

6.1. Kinetostatics performances and optimal design

Equation (15) can be exploited to deduce the relationship between the four-tuple $\tau = (\tau_1, \tau_2, \tau_3, \tau_4)^T$ that collects the generalized forces applied by the actuators and the wrench $(\mathbf{f}^T, \mathbf{m}^T)^T$ the platform

https://doi.org/10.1017/S0263574718000899 Published online by Cambridge University Press

applies to the external world as follows [5]. Actually, the power balance on the SMG (i.e., $\mathbf{f}^T\dot{\mathbf{A}}_1 + m_z\dot{\alpha} = \tau^T\dot{\mathbf{q}}$) together with Eq. (15) yield the following input-output static (StI/O) relationship:

$$\mathbf{J}^{-T}(\mathbf{f}^T, m_z)^T = \tau \tag{21}$$

with $\mathbf{J}^{-T} = \mathbf{N}^T\mathbf{M}^{-T} \equiv [\begin{matrix}\mathbf{U}_f & \mathbf{u}_\alpha \\ \mathbf{v}_f^T & v_\alpha\end{matrix}]$, where

$$\mathbf{U}_f = \begin{bmatrix} 1 & \dfrac{A_{2x}\sin\alpha}{A_{1y}\sin\alpha + A_{2x}\cos\alpha} & \dfrac{-A_{1y}A_{2x}\sin\alpha}{A_{1z}\left(A_{1y}\sin\alpha + A_{2x}\cos\alpha\right)} \\ 0 & \dfrac{d_2\sin\alpha}{A_{1y}\sin\alpha + A_{2x}\cos\alpha} & \dfrac{d_2A_{2x}\cos\alpha}{A_{1z}\left(A_{1y}\sin\alpha + A_{2x}\cos\alpha\right)} \\ 0 & \dfrac{A_{2x}\cos\alpha}{A_{1y}\sin\alpha + A_{2x}\cos\alpha} & \dfrac{-A_{1y}A_{2x}\cos\alpha}{A_{1z}\left(A_{1y}\sin\alpha + A_{2x}\cos\alpha\right)} \end{bmatrix}, \quad \mathbf{u}_\alpha = \begin{pmatrix} \dfrac{A_{2x}}{L\left(A_{1y}\sin\alpha + A_{2x}\cos\alpha\right)} \\ \dfrac{d_2}{L\left(A_{1y}\sin\alpha + A_{2x}\cos\alpha\right)} \\ \dfrac{-A_{1y}}{L\left(A_{1y}\sin\alpha + A_{2x}\cos\alpha\right)} \end{pmatrix}$$

$$\mathbf{v}_f^T = \left(0, \quad \frac{-d_4\sin\alpha}{A_{1y}\sin\alpha + A_{2x}\cos\alpha}, \quad \frac{d_4A_{1y}\sin\alpha}{A_{1z}\left(A_{1y}\sin\alpha + A_{2x}\cos\alpha\right)} \right), \qquad v_\alpha = \frac{-d_4}{L\left(A_{1y}\sin\alpha + A_{2x}\cos\alpha\right)}$$

The expansion of Eq. (21) transforms it as follows:

$$\mathbf{U}_f\mathbf{f} + \mathbf{u}_\alpha m_z = (\tau_1, \tau_2, \tau_3)^T, \tag{22a}$$

$$\mathbf{v}_f{}^T\mathbf{f} + v_\alpha m_z = \tau_4. \tag{22b}$$

Equation (22b) allows the linear elimination of m_z from Eq. (22a) which becomes as follows:

$$\mathbf{f} = \mathbf{J}_f\tau, \tag{23}$$

where $\mathbf{J}_f = \mathbf{E}^{-1}\mathbf{F}$ with $\mathbf{E} = [\mathbf{U}_f\text{–}(\mathbf{u}_\alpha\mathbf{v}_f^T/v_\alpha)]$, $\mathbf{F} = [\mathbf{1}_{3x3}, \text{–}\mathbf{u}_\alpha/v_\alpha]$ and $\mathbf{1}_{3x3}$ is the 3x3 identity matrix. Equation (23) implicitly takes into account m_z and, with respect to Eq. (21), it has the advantage that both the input τ and the output $\mathbf{f}$ are homogenous vectors whose entries are all forces. Thus, the condition $\mathbf{f}\cdot\mathbf{f} = 1$ is dimensionally consistent and yields the following 4-D ellipsoid with the introduction of Eq. (23):

$$\tau^T\mathbf{J}_f{}^T\mathbf{J}_f\tau = 1, \tag{24}$$

which is dimensionally consistent, too.

The shape of ellipsoid (24) depends on the SMG configuration through $\mathbf{J}_f$. The semi-axes lengths of this ellipsoid are the inverse of the singular values [6] of $\mathbf{J}_f$. Also, the minimum, $\lambda_{\min}$, and maximum, $\lambda_{\max}$, lengths of the semi-axes of ellipsoid (24) at a given configuration correspond to the minimum and maximum values, respectively, of $|\tau|$ necessary to equilibrate a unit resultant force applied to the platform at that configuration. Therefore, the following local index, CI, can be adopted as a measure of the kinetostatic performance of the SMG at a given configuration:

$$\mathrm{CI} = \frac{\lambda_{\min}}{\lambda_{\max}}. \tag{25}$$

[5]Hereafter, $\mathbf{f} = (f_x, f_y, f_z)^T$ is the resultant force and $\mathbf{m} = (m_x, m_y, m_z)^T$ is the resultant moment about A_1 of the force system the platform applies to the external world.

[6]The "singular values" of a real matrix $\mathbf{A}$ are the square roots of the eigenvalues of the positive-semi-definite matrix $\mathbf{A}^T\mathbf{A}$. Also, the spectral norm of $\mathbf{A}$ is the square root of the largest eigenvalue of $\mathbf{A}^T\mathbf{A}$; thus, the spectral norm of $\mathbf{A}$ is equal to its largest singular value.

https://doi.org/10.1017/S0263574718000899 Published online by Cambridge University Press

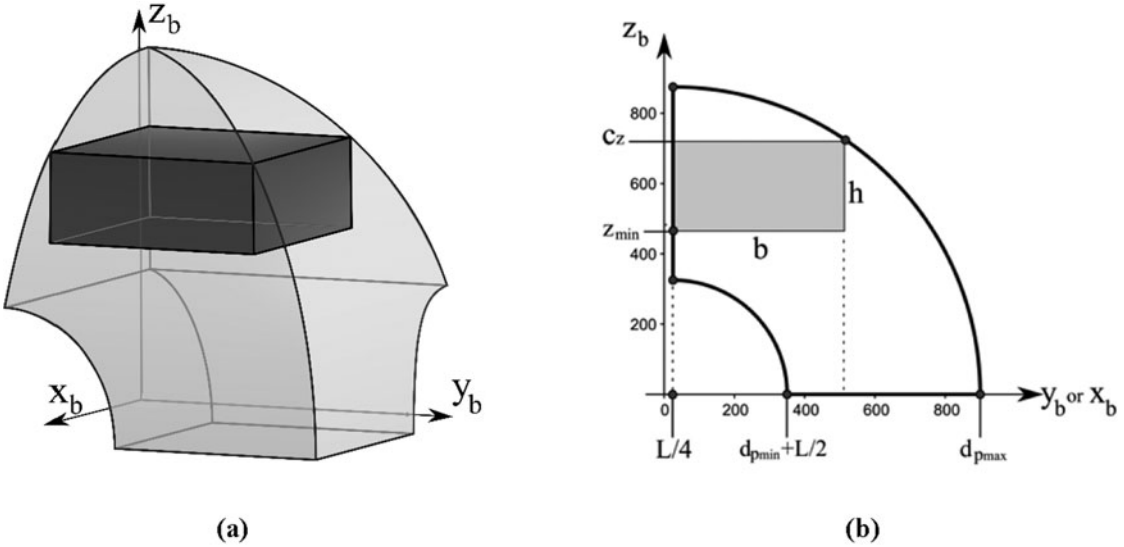

Fig. 13. Useful workspace with CI $\geq$ 0.45: (a) 3-D view (the useful workspace is the rectangular parallelepiped), and (b) projections onto the x_bz_b-and y_bz_b-planes (d_p corresponds to d_4 or d_2 for the x_bz_b or y_bz_b plane, respectively).

The above-defined CI ranges from 0 to 1: the higher the CI, the better the performance is. It corresponds to the conditioning index [27] of the Jacobian matrix $\mathbf{J}_f$ and can be used for any SMG. Accordingly, the global performance of the SMG can be measured by the global conditioning index [27], GCI, defined as the average value of CI on the useful workspace. Moreover, the concept of isotropic configuration [28] of an SMG can be referred to the SMG configurations with CI = 1.

Section 5 showed that, for the studied SMG, the geometric values $(d_{2max}/d_{2min}) = 3$, $u = 0.5$, $L = 100$ l.u., $d_{2min} = d_{4min} = 3\,L$ and $d_{2max} = d_{4max}$ provide a free-from-singularity dexterous workspace (Fig. 12) wide enough to locate a useful workspace adequate for industrial applications. For these geometric values, the CI values corresponding to the SMG configurations located in the dexterous workspace shown in Fig. 12 have been computed. This numerical analysis highlighted that the CI value increases with the z coordinate of O_e from $\mathrm{CI}_{\min} = 0$, at $z = 0$ (i.e., on the x_by_b plane), to the maximum value $\mathrm{CI}_{\max} = 0.707$. According to this computation, the useful workspace of the studied SMG must be located in the upper part of its dexterous workspace (Fig. 12) to get good kinetostatic performances.

The useful workspace is a regular geometric object (e.g., a cube, a ball, etc.)[29] located in the region of the operational workspace that satisfies all the kinetostatics requirements (e.g., CI $\geq \mathrm{CI}_{\min}$). Here, the useful workspace is chosen equal to the rectangular parallelepiped [see Fig. 13(a)] with maximum volume, V_u, that has a square base and two equal rectangular sides lying on the boundary surfaces of the dexterous workspace shown in Fig. 12. Figure 13(b) shows simultaneously its projections on the x_bz_b and y_bz_b planes with d_p that corresponds to d_4 or d_2 for the x_bz_b or y_bz_b plane, respectively. With reference to Fig. 13, $z_{\min}$ depends on the assigned minimum value, $\mathrm{CI}_{\min}$, of CI and the value reported in Fig. 13 corresponds to $\mathrm{CI}_{\min} = 0.45$. Once $\mathrm{CI}_{\min}$ is assigned the above-defined useful workspace is uniquely determined and, over $z_{\min}$, the maximum value, $\mathrm{CI}_{\max}$, and the average value, GCI, of CI in the useful workspace can be computed together with the volumetric ratio, V_u/V_o, between the volumes of the useful and the dexterous workspaces. Figure 14 shows a dimensionless diagram that, for each value of $z_{\min}/L$, gives the values of V_u/V_o, $\mathrm{CI}_{\max}$, $\mathrm{CI}_{\min}$ and GCI in the useful workspace.

The diagram of Fig. 14 shows that the GCI has always values greater than 0.602 (i.e., near to $\mathrm{CI}_{\max} = 0.707$), whereas $\mathrm{CI}_{\min}$ and V_u/V_o strongly depend on $z_{\min}/L$ with $\mathrm{CI}_{\min}$ that is always greater than 0.332 and V_u/V_o that is always lower than 34.4%. Such high GCI brings to conclude that only small parts of the useful workspace have CI values near to $\mathrm{CI}_{\min}$. A good compromise could be $\mathrm{CI}_{\min} = 0.45$ (i.e., the value of Fig. 13) since it yields $z_{\min} = 4.54$ L, $h = 2.24$ L, $b = 5.52$ L, $(V_u/V_o) = 20.9\%$ and GCI = 0.639, which are values interesting for practical applications (see Fig. 13).

https://doi.org/10.1017/S0263574718000899 Published online by Cambridge University Press

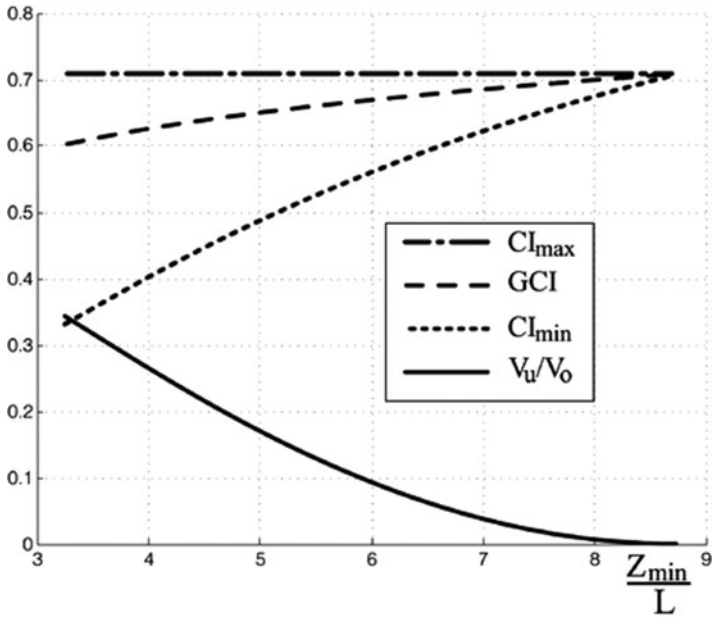

Fig. 14. Diagrams of V_u/V_o, CI_{min}, CI_{max} and GCI as a function of z_{min}/L.

7. Conclusions

Based on a previously identified 2PRPU topology, a novel SMG has been presented and studied. The novel SMG has a rotation amplifier that makes its end effector perform a complete rotation even though the platform, on which the end effector is hinged, can only perform a bounded rotation. The proposed SMG has a single-loop not-overconstrained architecture with actuators on or near the base.

The position analysis, the instantaneous kinematics and the workspace analysis of this SMG have been addressed. In particular, both the inverse (IPA) and the direct (DPA) position analyses have been solved in closed form. The IPA has only one solution that can be computed with simple formulas, whereas the DPA has up to eight real solutions symmetrically disposed with respect to a plane fixed to the base, which can be computed in closed form. A simple geometric construction has been devised to find and visualize all the DPA real solutions.

Regarding the instantaneous kinematics, the instantaneous input–output relationship has been deduced and the singularity analysis has been exhaustively addressed. Both analytical expressions of the singularity loci and a graphical tool that easily identifies singular configurations have been provided. The singularity analysis showed that the proposed SMG has no constraint singularity, and two type-II[19] singularity conditions; nevertheless, by bounding the platform rotation, wide operational-space regions that are FFS can be identified.

Eventually, the workspace analysis brought to determine the values of the geometric parameters that make the FFS dexterous workspace wide enough for including useful workspace suitable for real applications. The kinetostatics performances and the optimal location of the useful workspace of the proposed SMG have been discussed by using the so-obtained values of the geometric parameters.

All the above-summarized results highlight that the proposed SMG is a valid design alternative.

Acknowledgements

This work has been developed at the Laboratory of Advanced Mechanics (MECH-LAV) of Ferrara Technopole, supported by FIR2016 and FAR2017 funds, by Regione Emilia Romagna (District Councillorship for Productive Assets, Economic Development, Telematic Plan) POR-FESR 2007–2013, Attività I.1.1, and by CNPq – Conselho Nacional de Desenvolvimento Científico e Tecnológico (National Council for Scientific and Technological Development) -Project nº 232250/2014-6 - Brazil.

References

1. J. M. Hervé, "The lie group of rigid body displacements, a fundamental tool for mechanism design," *Mech. Mach. Theory* **34**, 719–730 (1999).
2. C.-C. Lee and J. M. Hervé "Type synthesis of primitive schoenflies-motion generators," *Mech. Mach. Theory* **44**, 1980–1997 (2009).
3. C.-C. Lee and J. M. Hervé "Isoconstrained parallel generators of schoenflies motion," *ASME J. Mech. Rob.* **3**(2), 021006-(1–10) (2011).
4. F. Pierrot and O. Company, "H4: A New Family of 4-DOF Parallel Robots," *Proceedings of the 1999 IEEE/ASME International Conference on Advanced Intelligent Mechatronics AIM'99*, Atlanta, Georgia, USA (1999) pp. 508–513.
5. S. Krut, O. Company, M. Benoit, H. Ota and F. Pierrot, "I4: A New Parallel Mechanism for SCARA Motions," *Proceedings of the 2003 International Conference on Robotics and Automation*, Taipei, Taiwan (2003) pp. 1875–1880.
6. V. Nabat, M. de la O Rodriguez, O. Company, S. Krut and F. Pierrot, "Par4: Very High Speed Parallel Robot for Pick-and-Place," *Proceedings of the 2005 IEEE/RSJ International Conference on Intelligent Robots and Systems* (2005) pp. 553–558.
7. J. Angeles, S. Caro, W. Khan and A. Morozov, "The design and prototyping of an innovative schoenflies motion generator," *Proc. IMechE-Part C: J. Mech. Eng.* **220**(C7), 935–944 (2006).
8. Z. Li, Y. Lou, Y. Zhang, B. Liao and Z. Li, "Type synthesis, kinematic analysis, and optimal design of a novel class of schoenflies-motion parallel manipulators," *IEEE Trans. Aut. Sc. Eng.* **10**, 674–686 (2013).
9. X. Kong and C. M. Gosselin, "Type synthesis of 3T1R 4-dof parallel manipulators based on screw theory," *IEEE Trans. Rob. Autom.* **20**, 181–190 (2004).
10. O. Company, F. Pierrot, V. Nabat and M. Rodriguez, "Schoenflies Motion Generator: A New Non Redundant Parallel Manipulator with Unlimited Rotation Capability," *Proceedings of the 2005 IEEE International Conference on Robotics and Automation*, Barcelona, Spain (2005) pp. 3250–3255.
11. P.-L. Richard, C. M. Gosselin and X. Kong "Kinematic analysis and prototyping of a partially decoupled 4-DOF 3T1R parallel manipulator," *ASME J. Mech. Des.* **129**, 611–616 (2007).
12. ABB, "IRB 360 – FlexPicker: Faster processing, faster payback," ABB Packaging Magazine, ABB Robotics, Issue: May 2008, p. 25 2008, (https://library.e.abb.com/public/aed4c1b308bc9fc2c1257456004f8734/EN_25_techpages_irb360_korr2_abb_pack_108.pdf).
13. M. Carricato, "Fully isotropic four-degrees-of-freedom parallel mechanisms for Schoenflies motion," *Int. J. Robot. Res.* **24**(5), 397–414 (2005).
14. F. Pierrot, O. Company, S. Krut and V. Nabat, "Four-Dof PKM with Articulated Travelling-Plate," *PKS'06: Parallel Kinematics Seminar*, Chemnitz, Germany (2006) pp. 25–26.
15. R. S. Ball *A Treatise on the Theory of Screws* (Cambridge University Press, Cambridge, UK, 1900, Reprinted in 1998).
16. J. E. Shigley and J. J. Uicker, *Theory of Machines and Mechanisms*," 2nd ed. (McGraw-Hill, Inc., New York, USA, 1995).
17. L. Euler, "Of a New Method of Resolving Equations of the Fourth Degree," **In**: *Elements of Algebra*, (Springer-Verlag, New York, Reprinted in 1984 from the 5th Edition of the 1st English translation published by Longman, London, UK, 1822) pp. 282–288 ISBN: 978-1-4613-8511-0
18. D. Zlatanov, I. A. Bonev and C. M. Gosselin, "Constraint Singularities of Parallel Mechanisms," *Proceedings of the 2002 IEEE International Conference on Robotics and Automation ICRA2002*, Washington, DC (2002) pp. 496–502.
19. C. M. Gosselin and J. Angeles, "Singularity analysis of closed-loop kinematic chains," *IEEE Trans. Robot. Autom.* **6**(3), 281–290 (1990).
20. O. Ma and J. Angeles, "Architecture Singularities of Platform Manipulators," *Proceedings of the 1991 IEEE International Conference on Robotics and Automation*, Sacramento CA, USA (1991) pp. 1542–1547.
21. D. Zlatanov, R. G. Fenton and B. Benhabib, "A unifying framework for classification and interpretation of mechanism singularities," *ASME J. Mech. Des.* **117**(4), 566–572 (1995).
22. C. D. Meyer, "Matrix analysis and applied linear algebra," *Soc. Ind. Appl. Math*. (SIAM, Philadelphia, PA, 2000) ISBN: 978-0-898714-54-8.
23. B. Siciliano, L. Sciavicco, L. Villani and G. Oriolo, *Robotics: Modelling, Planning and Control* (Springer-Verlag, London, 2009) p. 85, ISBN: 978-1-84628-641-4.
24. C. Gosselin, "Stiffness mapping for parallel manipulators," *IEEE Trans. Robot. Autom.* **6**(3), 377–382 (1990).
25. G. Wu, "Stiffness analysis and optimization of a co-axial spherical parallel manipulator," *Modeling, Identification Control* **35**(1), 21–30 (2014).
26. T. Harada and J. Angeles, "Kinematics and singularity analysis of a CRRHHRRC parallel Schönflies motion generator," *CSME Trans.* **38**(2), 173–183 2014.
27. C. Gosselin and J. Angeles, "A global performance index for the kinematic optimization of robotic manipulators," *J. Mech. Des.* **113**(3), 220–226 1991.
28. J. Angeles, "*Fundamentals of Robotic Mechanical Systems*, (Springer-Verlag, New York, 2014) ISBN: 978-3-319-30762-6.
29. Y. Lou, G. Liu, N. Chen and Z. Li, "Optimal Design of Parallel Manipulators for Maximum Effective Regular Workspace," *Proceedings of the 2005 IEEE/RSJ International Conference on Intelligent Robots and Systems*, Edmonton, Canada (2005) pp. 795–800.
30. P. Lee and J. Lee, "On the kinematics of a new parallel mechanism with Schoenflies motion," *Robotica* **34**(9), 2056–2070 (2016), DOI: 10.1017/S0263574714002732